A Multi-time Scale Tie-line Energy and Reserve Allocation Model Considering Wind Power Uncertainties for Multi-area Systems

Jian Xu, *Senior Member, IEEE, Member, CSEE*, Siyang Liao, *Member, CSEE*, Haiyan Jiang, Danning Zhang, Yuanzhang Sun, *Senior Member, IEEE*, Deping Ke, Xiong Li, Jun Yang, Xiaotao Peng, and Liangzhong Yao, *Senior Member, IEEE*

***Abstract*—Continued expansion of the power grid and the increasing proportion of wind power centralized integration leads to requirements in sharing both energy and reserves among multiple areas under a hierarchical control structure, which successively requires a correction between schedule plans within multi-time scale. In order to address this problem, this paper develops an information integration method integrating complicated relationships among fuel cost, total thermal power output, reserve capacity, owned reserves and expectations of load shedding and wind curtailment, into three types of time-related relationship curves. Furthermore, a multi-time scale tie-line energy and reserves allocation model is proposed, which contains two levels in the control structure, two time scales in dispatch sequence and multiple areas integrated within wind farms as scheduling objects. The efficiency of the proposed method is tested in a 9-bus test system and IEEE 118-bus system. The results show that a cross-regional control center is able to approach the optimal scheduling results of the whole system with the integrated uploaded relationship curves. The proposed model not only relieves energy and reserve shortages in partial areas but also allocates them to more urgent need areas in a high effectivity manner in both day-ahead and intraday time scales.**

***Index Terms*—Energy and reserve allocation, hierarchical control structure, multi-area system, multi-time scale economic dispatch, wind power.**

I. Introduction

LARGE-scale integration of wind power introduces new challenges to power systems combined with inherent characteristics in China [1]. The power systems in China are relatively large, including six regional power grids. Each regional power grid consists of several interconnected provincial power grids [2]. In order to ensure the safe operation of such a large power system, it is necessary to have a hierarchical control system [3]. Also, the wind power clusters are centrally integrated into the northwest of China, which is far away from the load centers [4]. Eight large-scale wind power bases have been created with more than 90 GW total capacity [5]. Hence, cross-regional co-optimization of both energy and reserve has become a trend in China [6]–[8]. Moreover, a multi-time scale coordination framework (MSCF) is already implemented in China to successively eliminate scheduling errors as time goes on [9].

This paper is influenced by the practical requirements in multi-time scale economic dispatch (ED) for a multi-area system with multi-wind-farms integrated into a hierarchical control structure. The inherent characteristics of China mentioned above bring relevant distinctiveness to this issue. First, the hierarchical control system brings problems of information security and different optimization objects into the upper control center (UCC) and local control center (LCC). As for China, the UCC owns the information of tie-lines connecting areas and schedules the boundary exchange quantities for each area. However, without knowing the tie-line information and schedule results for other areas, the LCC of each provincial power grid independently schedules the inside units to achieve an optimal benefits solution of its own area under the boundary shared energy and reserves already set by the UCC [10]. The relationship between the UCC and LCCs is presented in Fig. 1. Under China's vertical dispatch system, each regional power grid contains several provincial power grids connected by inter-provincial links. The regional power grid company has the line parameters and scheduling control authority of the inter-provincial contact line, which is used to optimize and dispatch the power and reserve interaction between the provinces. Regional grid companies do not dispatch specific units in each province, nor can they obtain the parameters of units and lines in the province. According to the specific parameters of the province's generating units, i.e., the provincial transmission line parameters and the province's transmission grid structure, the provincial power grid companies will take the province's best economic scenario as the dispatching target, and optimize the dispatch of the power generating units in the province based on the determined interactive power and reserve plans.

Manuscript received March 1, 2020; revised May 27, 2020; accepted June 10, 2020. Date of online publication July 6, 2020; date of current version September 28, 2020. This work was supported in part by the Science and Technology Project of Central Branch of SGCC (SGHZ0000DKJS1900228) and in part by the National Natural Science Foundation of China (51707136).

J. Xu (ORCID: https://orcid.org/0000-0002-7673-2887) , S. Y. Liao (corresponding author, e-mail: liaosiyang@whu.edu.cn; ORCID: https://orcid.org/0000-0002-4092-764X), Y. Z. Sun, D. P. Ke, X. Li, J. Yang, X. T. Peng and L. Z. Yao are with the School of Electrical Engineering and Automation, Wuhan University, Wuhan 430072, China.

H. Y. Jiang is with State Grid (Suzhou) City & Energy Research Institute, Suzhou 215000, China.

D. N. Zhang is with State Grid Zhengzhou Electric Power Supply Company, Zhengzhou 450000, China.

DOI: 10.17775/CSEEJPES.2020.00620

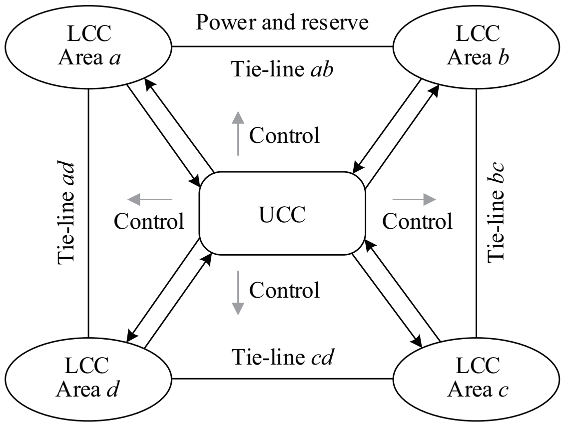

Fig. 1. Vertical scheduling relationship and information exchange process between the UCC and LCCs.

The provincial power grid needs to keep the unit and line parameters in the province confidential and only upload the interactive information among the provinces to the regional dispatch. Thus, the issue of how to realize the optimal tie-line scheduling in the UCC on the basis of ensuring the LCC's information privacy needs to be studied. Second, the energy and reserve sharing among areas are supposed to ease both power fluctuation and reserve shortages of the installed systems with large-scale wind power bases [11]. Therefore, it is worth considering how to evaluate which areas have a greater urgency for energy and reserves when wind power is integrated in more than one area [12] and how to arrange the providers of energy and reserves under the existing grid structure [13]. Third, within the MSCF, updated forecasts during a multi-time scale can lead to new power imbalances and an updated forecast error distribution leads to updated reserve demands in the areas [9], [14]. Hence, both energy and reserves are needed to correct the intraday look-ahead time scale.

To solve the coordination of multiple LCCs, [2] describes a decentralized approach based on a modified generalized benders decomposition. In [6] a fully decentralized optimization is implemented based on the cutting plane consensus algorithm. In [12] the boundary phase angles of each area are chosen as coupling variables and are able to obtain a solution by iterating between the LCCs and UCC. In [15] an augmented Lagrange algorithm relies on no UCC being required, but just moderate interchanges of information among LCCs.

All the references above except [12] adopt algorithms which mathematically decentralize the original problems and coordinate the sub-problems in multiple iterations which require substantial data exchange among the LCCs. In these methods, synchronous information interaction with high communication costs or slow rates of convergence happen since no UCC is considered [16]. However, the UCCs and LCCs in China have their different but clear responsibilities, which make these methods no longer applicable for China. Moreover, all these references only consider the tie-line energy dispatch without co-optimizing energy and reserves together. This may cause reserves being unavailable when needed from other areas.

For the third problem under this background, [10] formulates the coordinated tie-line scheduling problem by using a two-stage adaptive robust optimization and explicates the relationships of inputs and outputs belonging to different time scales in the MSCF. Similarly, [14] also develops a MSCF for quantifying regulation service requirements, and a multi-time-scale method is considered for quantifying regulation service requirements considering the combined impact of wind variations. Although the above references can contribute to the ED problem in MSCF, only [10] studies this issue in a multi-area system. Also, [14] ignores the day-ahead scheduling part in the MSCF. In general, none of them consider the reserve shared along with the energy together among areas and all of them are not suitable for the hierarchical control structure adopted in multi-area systems.

This paper proposes an information integration method for a regional grid and a hierarchical scheduling model across both time and space. The major contributions of this paper are summarized as follows:

1) An information integration method is developed for a regional power grid. This method integrates complicated relationships among total thermal power output, fuel costs, reserve capacity, owned reserve volume and expectations of load shedding (LS) and wind curtailment (WC) into three types of time-related curves representing each area. Furthermore, the developed method not only protects regional information privacy, but also provides sufficient information for a cross-region control center to achieve a high quality solution compared with the condition of omniscient information.

2) A multi-time scale scheduling model is designed to allocate energy and reserve resources with high efficiency among both dispatch periods and areas. Moreover, the proposed model includes a multi-control-level to adapt to the hierarchical control structure and includes multi-time scale sub-models to correct the day-ahead scheduling results based on the intraday look-ahead forecast information achieving lower operational costs for the whole system.

The remainder of this paper is organized as follows. In Section II, an information integration method is developed. In Section III, a multi-time scale tie-line energy and reserve allocation (TERA) model is proposed. In Section IV, the proposed information integration method and multi-time scale TERA model are both tested in a 9-bus test system and the IEEE 118-bus system. Section V summarizes the conclusions.

II. Information Integration Process in a LCC

As with an UCC, it needs to know the answers to three questions in order to achieve the results of power resource sharing and efficient distribution within the whole system. First, which area provides power with lower cost? Second, how does the change in total output of an area affect the change in its ability to provide upward or downward reserve? Third, how does the change in the provision of upward or downward reserve of an area affect the change in LS or WC expectations in the area? To solve the above three questions, this paper proposes three types of information integration curves.

A. Relationship of Total Thermal Power Outputs and Total Fuel Costs

Suppose that there are three thermal units in an area and their consumption characteristic curves can be represented by F_{th1}, F_{th2}, and F_{th3} in (1). The tangent slope of any point on these consumption characteristic curves is the incremental consumption rate λ. According to the Equal Incremental Principle [17], the total fuel consumption will be minimized if the incremental consumption rates of the three units are all in the same dispatch period, $\lambda_1 = \lambda_2 = \lambda_3 = \lambda$. Therefore, the relationship between the power outputs of the thermal units and λ can be obtained as shown in (2).

$$F_i^{\text{th}} = a_i + b_i P_{i,t}^{\text{th}} + c_i (P_{i,t}^{\text{th}})^2, \quad i = 1, 2, 3 \tag{1}$$

$$P_{1,t}^{\text{th}} = \frac{\lambda - b_1}{2c_1}, \; P_{2,t}^{\text{th}} = \frac{\lambda - b_2}{2c_2}, \; P_{3,t}^{\text{th}} = \frac{\lambda - b_3}{2c_3} \tag{2}$$

where a_i, b_i and c_i are the consumption coefficient of the ith thermal power unit, and $P_{i,t}^{\text{th}}$ is the power outputs of ith thermal unit in the tth dispatch period.

Besides the relationship presented in (2), power outputs of thermal units are also constrained by (3) and (4). Constraint (3) shows the upper and lower bounds for power output of thermal unit i. Constraint (4) is the ramping capacity constraint, in which R_i^U and R_i^D are the maximum output increase and decrease of thermal unit i during a dispatch period.

$$P_i^{\text{th,min}} \leqslant P_{i,t}^{\text{th}} \leqslant P_i^{\text{th,max}} \tag{3}$$

$$-R_i^D \leqslant (P_{i,t+1}^{\text{th}} - P_{i,t}^{\text{th}}) \leqslant R_i^U \tag{4}$$

Hence, the curves with unit power outputs as the abscissas and λ as the ordinate can be plotted as shown in Fig. 2(a). Furthermore, the integrated curve reflects the relationship between the total output of thermal units within this area and λ is shown on the right. And the total thermal output has a corresponding range of changes in a certain dispatch period corresponding to (3) and (4). Therefore, if $P_{1,t}^{\text{th}}$, $P_{2,t}^{\text{th}}$, $P_{3,t}^{\text{th}}$ within this area are all known, the total fuel cost in this area can be directly calculated. The relationship curve describing the relationship of total power outputs of thermal units and total fuel cost within an area is shown in the yellow part in Fig. 2 (a). This relationship is named as $P_{m,t}^C$. In Fig. 2(a), $P_{m,t}^{\text{total}}$ is the total thermal power output of area m; C_m^{Fuel} is the corresponding total fuel cost of area m; Curve ΔP_x^C is the variation form of $P_{m,t}^C$ which describes the relationship between $\Delta P_{m,t}^{\text{total}}$ and ΔC_m^{Fuel} at the point x on $P_{m,t}^C$. ΔP_x^C is appropriate for the correction process described later in Section III.

B. Relationship of Total Thermal Power Outputs and Total Reserve Capabilities

The second type is named as $P_{m,t}^{\text{Rup}}$ and $P_{m,t}^{\text{Rdn}}$, indicating the relationship of total thermal power outputs with total upward and downward reserve capabilities within one area respectively. The derivative processes of the relationship curve $P_{m,t}^{\text{Rup}}$ and $P_{m,t}^{\text{Rdn}}$ are shown in the blue part of Fig. 2(a) according to (5). Equation (5) explains that total upward reserve capability $\bar{r}_{m,t}^{\text{th}}$ and downward reserve capability $\underline{r}_{m,t}^{\text{th}}$ held by area m are the sum of each thermal unit's reserve

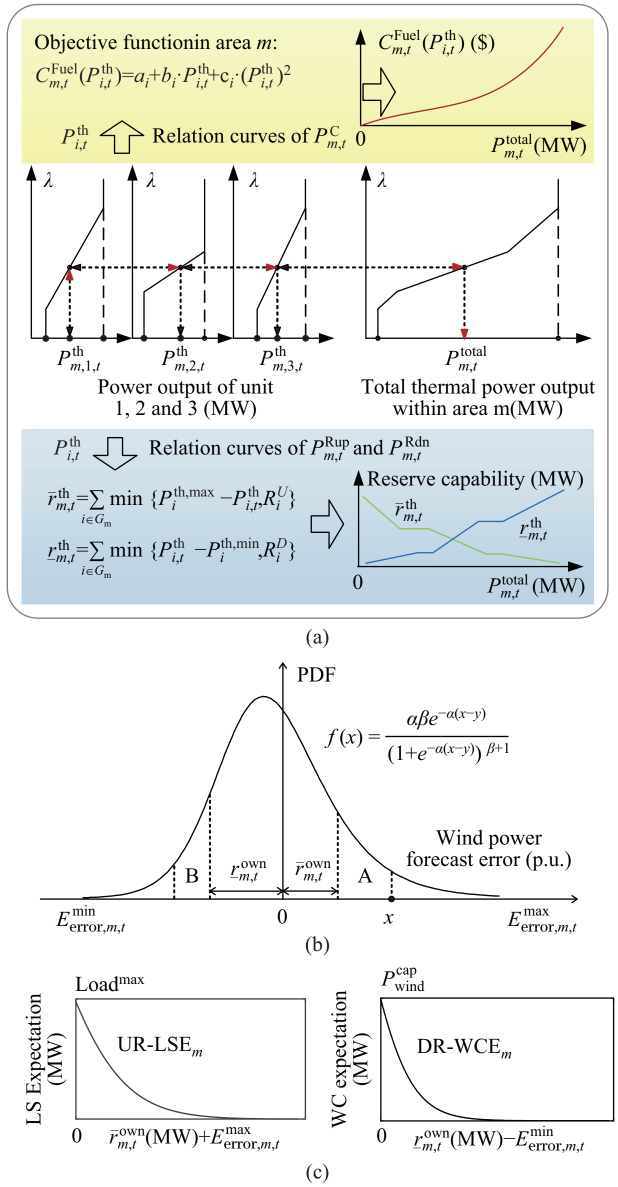

Fig. 2. Derivation processes of three types of relationship curves. (a) Derivation processes of the relationship curves of $P_{m,t}^C$, $P_{m,t}^{\text{Rup}}$ and $P_{m,t}^{\text{Rdn}}$. (b) Illustration of wind power forecast error probability distribution in a certain bin. (c) Illustration of $R_{m,t}^{\text{LS}}$ and $R_{m,t}^{\text{WC}}$ under a certain dispatch period with the corresponding wind power forecast value.

capacity after considering its ramp capability. $P_{m,t}^{\text{Rup}}$ and $P_{m,t}^{\text{Rdn}}$ express the relationship of $P_{m,t}^{\text{Rdn}}$ and provide for the capacity of the upward or downward reserve. ΔP_x^{Rup} and ΔP_x^{Rdn} are the variation forms of $P_{m,t}^{\text{Rup}}$ and $P_{m,t}^{\text{Rdn}}$.

$$\begin{aligned} \bar{r}_{m,t}^{\text{th}} &= \sum_{i=1,2,3} \min\left\{P_i^{\text{th,max}} - P_{i,t}^{\text{th}}, R_i^U\right\} \\ \underline{r}_{m,t}^{\text{th}} &= \sum_{i=1,2,3} \min\left\{P_{i,t}^{\text{th}} - P_i^{\text{th,min}}, R_i^D\right\} \end{aligned} \tag{5}$$

C. Relationship of Reserve Capabilities and Their Benefits

At last, the relationship curves named as $R_{m,t}^{\text{LS}}$ and $R_{m,t}^{\text{WC}}$ are developed to integrate the relationship of the total reserve capability held by a certain area and the LS/WC expectations within this area. Since improper reserve capacity leads to LS and WC in a system, we use expectations of LS and WC to measure the effect of owning upward reserve and downward reserve, and thus (6) and (7) are derived in this paper to describe these relationships. According to [18], the LS incident happens when the wind power forecast error is greater than the upward reserve owned by this area and WC happens when the absolute value of the wind power forecast error is greater than the downward reserve owned by this area. $f_{m,t}(x)$ in (8) is the probability distribution function (PDF) of the versatile probability distribution (VPD) [19] which is presented in Fig. 2(b) and is adopted to fit the distribution of the historical wind power forecast error of area m. The amount of LS is (x-$\bar{r}^{\text{own}}_{m,t}$) and the corresponding probability of this LS incident is $f_{m,t}(x)$ when the wind power forecast error x is greater than $\bar{r}^{\text{own}}_{m,t}$. Therefore, the expectation of LS under certain forecast values is the integral of (x-$\bar{r}^{\text{own}}_{m,t}$)$\times$ $f_{m,t}(x)$ from $\bar{r}^{\text{own}}_{m,t}$ to $E^{\max}_{\text{error, m, t}}$ is the maximum wind power forecast error which ever appeared in the historical data assembled in a certain bin corresponding to a forecast level of area m. Analogously, the expectation of WC under certain forecast values is the integral of (-$\underline{r}^{\text{own}}_{m,t}$-$x$) $\times$ $f_{m,t}(x)$ from $E^{\min}_{\text{error, m, t}}$ to (-$\underline{r}^{\text{own}}_{m,t}$) as shown in (7). $R^{\text{LS}}_{m,t}$ expresses the relationship of the "upward reserve owned by area m" and the "LS expectation estimated in area m." $R^{\text{WC}}_{m,t}$ expresses the relationship of the "downward reserve owned by area m" and the "WC expectation estimated in area m."

$$\mathrm{R}^{\text{LS}}_{m,t}(\bar{r}^{\text{own}}_{m,t}) = \int_{\bar{r}^{\text{own}}_{m,t}}^{E^{\max}_{\text{error, m, t}}} (x-\bar{r}^{\text{own}}_{m,t}) f_{m,t}(x)\mathrm{d}x \tag{6}$$

$$\mathrm{R}^{\text{WC}}_{m,t}(\underline{r}^{\text{own}}_{m,t}) = \int_{-\underline{r}^{\text{own}}_{m,t}}^{E^{\min}_{\text{error, m, t}}} (x+\underline{r}^{\text{own}}_{m,t}) f_{m,t}(x)\mathrm{d}x \tag{7}$$

$$f_{m,t}(x|\alpha_{m,t},\beta_{m,t},\gamma_{m,t}) = \frac{\alpha_{m,t}\beta_{m,t}\mathrm{e}^{-\alpha_{m,t}(x-\gamma_{m,t})}}{(1+\mathrm{e}^{-\alpha_{m,t}(x-\gamma_{m,t})})^{\beta_{m,t}+1}} \tag{8}$$

where $\alpha_{m,t}$, $\beta_{m,t}$ and $\gamma_{m,t}$ are the shape parameters of VPD within area m in dispatch period t.

However, (6) and (7) are not conducive to be applied directly since $\mathrm{R}^{\text{LS}}_{m,t}(\bar{r}^{\text{own}}_{m,t})$ and $\mathrm{R}^{\text{WC}}_{m,t}(\bar{r}^{\text{own}}_{m,t})$ are non-explicit integral functions. Thus, the independent variables $\bar{r}^{\text{own}}_{m,t}$ and $\bar{r}^{\text{own}}_{m,t}$ are evenly separated into 1000 points within the possible range of values in each bin. And the numerical integration method [20] is adopted to get the corresponding function values. The final relationship curves are presented in Fig. 2(c). Also, there are the variation forms of this type of relationship curves, namely the ΔR^{LS}_{x} and ΔR^{WC}_{x}.

III. Multi-time Scale TERA Model in a Hierarchical Control Structure

A. Day-ahead TERA Model

The day-ahead TERA model is launched in a receding horizon of 24 h and determines boundary exchanged qualities in the UCC and generation outputs of all units in their LCCs in the following 24 h with a time resolution of 15 min.

1) Day-ahead TERA Model in the UCC

a) Objective function:

$$\begin{aligned} C^{\text{UCC}}_{\text{day\_ahead}} = &\sum_{m\in AREA}\sum_{t\in T}\mathrm{PC}_{m,t}(P^{\text{total}}_{m,t}) + \\ &\sum_{m\in AREA} C^{\text{LS}}_{m}\sum_{t\in T}\mathrm{RLS}_{m,t}(R^{\text{up}}_{m,t}-\tilde{R}^{\text{up}}_{m,t}) + \\ &\sum_{m\in AREA} C^{\text{WC}}_{m}\sum_{t\in T}\mathrm{RWC}_{m,t}(R^{\text{dn}}_{m,t}-\tilde{R}^{\text{dn}}_{m,t}) \end{aligned} \tag{9}$$

where C^{LS}_{m} and C^{WC}_{m} are the LS cost and the WC penalty cost of area m; $P^{\text{total}}_{m,t}$ is the total power output of area m in the dispatch period t; $R^{\text{up}}_{m,t}$ and $R^{\text{dn}}_{m,t}$ are the capability of providing upward and downward reserves; $\tilde{R}^{\text{up}}_{m,t}$ and $\tilde{R}^{\text{dn}}_{m,t}$ are the boundary upward and downward exchanged reserves by area m with other areas. UCC needs day-ahead integrated relationship curves from the LCCs to start the tie-line allocation among the areas.

b) Constraints:

$$R^{\text{up}}_{m,t} \leqslant P^{\text{Rup}}_{m,t}(P^{\text{total}}_{m,t}), R^{\text{dn}}_{m,t} \leqslant P^{\text{Rdn}}_{m,t}(P^{\text{total}}_{m,t}) \tag{10}$$

$$F^{-1}_{m,t}(\bar{c}_m) \leqslant R^{\text{up}}_{m,t}-\tilde{R}^{\text{up}}_{m,t}, -F^{-1}_{m,t}(1-c_m) \leqslant R^{\text{dn}}_{m,t}-\tilde{R}^{\text{dn}}_{m,t} \tag{11}$$

where $\bar{c}_m$ and $\underline{c}_m$ are related to the level of risk for LS and WC in the chance constraints; $F^{-1}_{m,t}(x)$ is VPD's inverse function of wind power forecast error's probability density function (CDF) of area m in t. The specific expression of $F^{-1}_{m,t}(x)$ is shown in (12) and (13).

$$F^{-1}_{m,t}(\bar{c}_m) = \gamma_{m,t} - \frac{1}{\alpha_{m,t}}\ln(\bar{c}_m^{-1/\beta_{m,t}}-1) \tag{12}$$

$$F^{-1}_{m,t}(1-\bar{c}_m) = \gamma_{m,t} - \frac{1}{\alpha_{m,t}}\ln\left[(1-\bar{c}_m)^{-1/\beta_{m,t}}-1\right] \tag{13}$$

Constraint (10) shows that reserve capabilities held by area m are affected by total thermal units' output within area m in t. Constraint (11) requires that the upward and downward reserve owned by area m is larger than the wind power forecast error in a certain confidence level $\bar{c}_m$ and $\underline{c}_m$.

c) Tie-line constraints for exchange energy and reserves:

$$L^{\min}_{l} \leqslant \sum_{m\in AREA} G^{\text{UCC}}_{m,l}\tilde{P}_{m,t} \leqslant L^{\max}_{l} \tag{14}$$

$$L^{\min}_{l} \leqslant \sum_{m\in AREA} G^{\text{UCC}}_{m,l}(\tilde{P}_{m,t}+\tilde{R}^{\text{up}}_{m,t}) \leqslant L^{\max}_{l} \tag{15}$$

$$L^{\min}_{l} \leqslant \sum_{m\in AREA} G^{\text{UCC}}_{m,l}(\tilde{P}_{m,t}-\tilde{R}^{\text{dn}}_{m,t}) \leqslant L^{\max}_{l} \tag{16}$$

where $\tilde{P}_{m,t}$ is the boundary power exchanged by area m with other areas; $G^{\text{UCC}}_{m,l}$ showss the generation shift distribution factor of the inject power of area m to the corresponding transmission line l. For the UCC, each area is equivalent to a node and the network is made up of all the cross-region tie-lines.

Constraint (14) is the constraint of tie-lines among areas using DC power flow. Constraint (15) and (16) require that the power flow, along with the exchange reserve, be together to meet the thermal stability constraints, which ensures that the cross regional shared reserve can be transmitted through the tie-lines.

d) Other balance constraints:

$$(P_{m,t}^{\text{total}} - \tilde{P}_{m,t}) + P_{m,t}^{\text{wind, DA}} = P_{m,t}^{\text{load}} \tag{17}$$

$$\sum_{m\in AREA} \tilde{P}_{m,t} = 0, \sum_{m\in AREA} \tilde{R}_{m,t}^{\text{up}} = 0, \sum_{m\in AREA} \tilde{R}_{m,t}^{\text{dn}} = 0 \tag{18}$$

where $P_{m,t}^{\text{wind, DA}}$ here is the day-ahead forecast value of the wind power of area m in dispatch period t.

Constraint (17) is the power balance constraint for each area. And all the energy and reserve shared among areas are supposed to be balanced in (18) since no extra energy could be generated in the tie-lines.

2) Day-ahead ED Model in the LCCs

Boundary exchange variables $\tilde{P}_{m,t}$, $\tilde{R}_{m,t}^{\text{up}}$ and $\tilde{R}_{m,t}^{\text{dn}}$, as well as $P_{m,t}^{\text{total}}$, $R_{m,t}^{\text{up}}$ and $R_{m,t}^{\text{dn}}$ assigned to area m are known quantities to the LCC within area m since they are already scheduled by the UCC. Each area can set specific constraints according to the characteristics of its own practical applications. Only the basic ED model for the LCC in area m is presented here as a reference.

a) Objective function:

$$C_{\text{day\_ahead, m}}^{\text{LCC}} = \sum_{i\in G_m}\sum_{t\in T}\left[a_i + b_i\cdot P_{i,t}^{\text{th}} + c_i\cdot (P_{i,t}^{\text{th}})^2\right] \tag{19}$$

where a_i, b_i and c_i are fuel cost parameters of unit i within area m; $P_{i,t}^{\text{th}}$ is the schedule output of thermal unit i within area m.

Equation (19) represents the fuel costs of thermal power units within area m.

b) Constraints:

$$\sum_{i\in G_m} P_{i,t}^{\text{th}} - \tilde{P}_{m,k,t} = P_{m,t}^{\text{total}} \tag{20}$$

$$L_l^{\min} \leqslant \sum_{k\in BUS_m} G_{k,l}^{\text{LCC}}(P_{k,t}^{\text{th}} + P_{k,t}^{\text{wind}} - \tilde{P}_{m,k,t} - D_{k,t}) \leqslant L_l^{\max} \tag{21}$$

$$\sum_{i\in G_m} \bar{r}_{i,t}^{\text{th}} = R_{m,t}^{\text{up}}, \sum_{i\in G_m} \underline{r}_{i,t}^{\text{th}} = R_{m,t}^{\text{dn}} \tag{22}$$

$$\bar{r}_{i,t}^{\text{th}} = \min\left\{P_i^{th,max} - P_{i,t}^{\text{th}}, RU_i\right\},$$
$$\bar{r}_{i,t}^{\text{th}} = \min\left\{P_{i,t}^{\text{th}} - P_i^{\text{th, min}}, RD_i\right\} \tag{23}$$

Constraint (20) guarantees the power balance within area m. $\tilde{P}_{m,k,t}$ is the boundary power exchanged by area m with other areas of bus k in dispatch period t. $P_{m,t}^{\text{total}}$ here is the input information from the UCC. Constraint (21) limits line capacity within area m. $G_{k,l}^{\text{LCC}}$ shows the generation shift distribution factor of the inject power of bus k to the corresponding line l within area m. $P_{k,t}^{\text{wind}}$ and $D_{k,t}$ here are the day-ahead forecast of wind power and load of bus k in t respectively. Constraint (22) guarantees the total upward and downward reserve in one area can be allocated to each unit. Reserve capacity constraints for unit i are shown in (23). In addition, (3) and (4) explained in Section II, should also be considered in the LCCs.

B. Look-ahead TERA Model

In addition to the variation form of the look-ahead integrated information from the LCCs, $P_{m,t}^{\text{error}}$ is also the input data which is the forecast error within area m caused by the look-ahead updated wind power information and is explained in (24). $P_{m,t}^{\text{wind, ID}}$ is the look-ahead wind power forecast. Moreover, the decision variables scheduled by the day-ahead TERA model are also the inputs for the start point of the look-ahead correction process. The look-ahead TERA model in the MSCF is launched in a receding horizon every 1 h and determines the generation outputs of all units in the upcoming 4 h, with a time resolution of 15 min.

$$P_{m,t}^{\text{error}} = P_{m,t}^{\text{wind, ID}} - P_{m,t}^{\text{wind, DA}} \tag{24}$$

1) Look-ahead TERA Model in the UCC

a) Objective function:

$$C_{\text{look\_ahead}}^{\text{UCC}} = \sum_{m\in AREA}\sum_{t\in T}\Delta P_{P_{m,t}^{\text{total, DA}}}^{C}(\Delta P_{m,t}^{\text{total}}) + \sum_{m\in AREA} C_m^{\text{LS}}\sum_{t\in T}\Delta R_{R_{m,t}^{\text{up, DA}}}^{\text{LS}}(\Delta R_{m,t}^{\text{up}} - \Delta\tilde{R}_{m,t}^{\text{up}}) + \sum_{m\in AREA} C_m^{\text{WC}}\sum_{t\in T}\Delta R_{R_{m,t}^{\text{dn, DA}}}^{\text{WC}}(\Delta R_{m,t}^{\text{dn}} - \Delta\tilde{R}_{m,t}^{\text{dn}}) \tag{25}$$

where $\Delta P_{m,t}^{\text{total}}$ is the total output *adjustment* made by the thermal units within area m in order to balance the total forecast error $P_{m,t}^{\text{error}}$; $\Delta R_{m,t}^{\text{up}}$ and $\Delta R_{m,t}^{\text{dn}}$ show the *adjustments* of the upward and downward reserve capabilities; $\Delta\tilde{R}_{m,t}^{\text{up}}$ and $\Delta\tilde{R}_{m,t}^{\text{dn}}$ show the adjustments of the upward and downward reserve shared with other areas.

The objective function (25) of the UCC in look-ahead time scale consists of three items. The first item shows the sum change of the thermal units' fuel costs within AREA throughout T. The second item shows the sum variations of the LS expectations within all areas throughout T. The third item shows the sum variations of WC expectations within all areas throughout T. Different from (9), (25) is supposed to minimize the total correction costs based on the day-ahead schedule results.

b) Additional constraints:

$$\Delta R_{m,t}^{\text{up}} \leqslant \Delta P_{P_{m,t}^{\text{total, DA}}}^{\text{Rup}}(\Delta P_{m,t}^{\text{total}}), \Delta R_{m,t}^{\text{dn}} \leqslant \Delta P_{P_{m,t}^{\text{total, DA}}}^{\text{Rdn}}(\Delta P_{m,t}^{\text{total}}) \tag{26}$$

Constraint (26) replaces (10) since the *variation forms* instead of the original forms of the relationship curves are adopted in the look-ahead dispatch model.

c) Explanations of the adjustment relationship:

$$P_{m,t}^{\text{error}} = \Delta P_{m,t}^{\text{total}} - \Delta\tilde{P}_{m,t} \tag{27}$$

$$\tilde{P}_{m,t} = \tilde{P}_{m,t}^{\text{DA}} + \Delta\tilde{P}_{m,t} \tag{28}$$

$$R_{m,t}^{\text{up}} = \Delta P_{P_{m,t}^{\text{total, DA}}}^{\text{Rup}}(0) + \Delta R_{m,t}^{\text{up}}$$
$$R_{m,t}^{\text{dn}} = \Delta P_{P_{m,t}^{\text{total, DA}}}^{\text{Rdn}}(0) + \Delta R_{m,t}^{\text{dn}} \tag{29}$$

$$\tilde{R}_{m,t}^{\text{up}} = \tilde{R}_{m,t}^{up,DA} + \Delta\tilde{R}_{m,t}^{\text{up}}, \tilde{R}_{m,t}^{\text{dn}} = \tilde{R}_{m,t}^{\text{dn, DA}} + \Delta\tilde{R}_{m,t}^{\text{dn}} \tag{30}$$

where $\Delta\tilde{P}_{m,t}$ is the adjustment of power that area m exchanges with other areas.

Constraint (27) shows that the power unbalance within area m is supposed to be covered by adjustments of both thermal units' output within this area and the exchanged power with other areas. Constraint (28) shows that the final boundary exchanged power of an area is the sum of its original day-ahead schedule and its look-ahead correction. Similarly, (29) shows this relationhip in upward and downward reserve capability. Constraint (30) shows this relationship of the upward and downward exchange reserve of area m with other areas.

2) Look-ahead ED Model in LCCs

$$C^{\text{LCC}}_{\text{look\_ahead, m}} = \sum_{i\in G_m}\sum_{t\in T}\left[a_i + b_i\left(P^{\text{th, DA}}_{i,t} + \Delta P^{\text{th}}_{i,t}\right) + c_i\left(P^{\text{th, DA}}_{i,t} + \Delta P^{\text{th}}_{i,t}\right)^2\right] \tag{31}$$

where $P^{\text{th, DA}}_{i,t}$ is the day-ahead scheduled power output of thermal unit i in dispatch period t; $\Delta P^{\text{th}}_{i,t}$ is the adjustment of the schedule output of thermal unit i within area m.

The proposed look-ahead TERA model within the multi-time scale TERA is summarized in (32) and (33), in which (32) shows the UCC part and (33) shows the LCCs part. All the optimizations in LCCs mentioned above are executed in parallel.

$$\begin{cases}\text{obj. (25)}\\ \text{st. (11)–(18), (24), (26)–(30)}\end{cases} \tag{32}$$

$$\begin{cases}\text{obj. (31)}\\ \text{st. (3)–(4), (20)–(23)}\end{cases} \tag{33}$$

C. Linearization Process of a Multi-time Scale TERA Model

The piecewise linear method in reference [21] is applied to the last two items of (9) and (25). The nonlinear functions $R^{\text{LS}}_{m,t}(\bar{r}^{\text{own}}_{m,t})$ and $R^{\text{WC}}_{m,t}(\underline{r}^{\text{own}}_{m,t})$ are therefore transformed into piecewise linear functions as shown in Fig. 3, which is much more friendly to the scheduling model. The $R^{\text{LS}}_{m,t}$ and $R^{\text{WC}}_{m,t}$ curves can describe the relationship between the reserved reserve in the area and its corresponding LS and WC expectations, which describe the effect of each area reserving reserve capacity in different scheduling periods. Based on this, the UCC will allocate upward and downward reserves efficiently among different areas.

IV. CASE STUDY

The proposed information integration method and the multi-time scale TERA model are both tested in a 9-bus test system

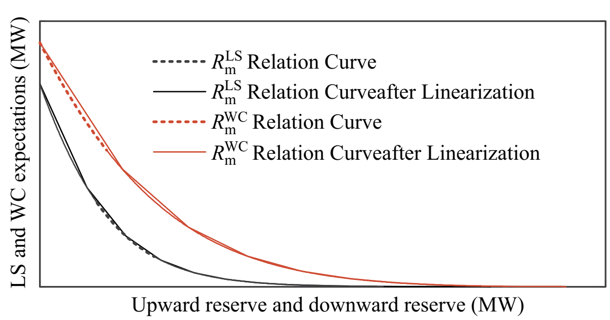

Fig. 3. Piecewise linear examples of the R^{LS}_m and R^{WC}_m in a certain bin.

and the IEEE 118-bus system [22]. The 9-bus test system is adopted to analyze effects of the proposed method in detail. Since the 118-bus system represents a portion of the Midwestern American Power System, it is used to verify the applicability of the model and strategy in an actual interconnected power system [23]. All the following results are demonstrated with the time scale of 16 dispatch periods in four hours, which shows the final results after a day-ahead TERA, and one round of a look-ahead TERA. The codes are executed on MATLAB software [24] based on an IBM CPLEX 12.4 solver [25].

A. The 9-bus Test System

1) System and Input Data

The 9-bus test system includes three wind farms and six thermal units distributed in three areas shown in Fig. 4(a). Wind farms integrated in bus 3, bus 6 and bus 9 are with 40 MW, 40 MW and 80 MW installed capacity respectively. The basic parameters of the thermal units are listed in Table I. The capacity limitations of the tie-lines are 100 MW. The ratio of loads in area 1, area 2 and area 3 are 30.10%, 28.80% and 40.10% respectively. Additionally, the unit penalty cost of the WC is set as 80 \$/(MW·h) [26], and the LS cost is set as 3500 \$/MW·h according to the Midwest ISO of USA [27]. It is worth noting that there is no need to consider the correlation among the three wind farms located in the three areas, because the three wind farms are located in three different areas, and the dispatching plans of the three areas are respectively formulated by their LCCs. Different LCCs do not interfere with each other's scheduling plan, and the output of the wind farms in area 1 will not affect the LCCs in area 2 and area 3 to formulate scheduling plans.

TABLE I
BASIC PARAMETERS OF THERMAL UNITS IN 9-BUS SYSTEM

Thermal Units	a_i	b_i	c_i	$P_i^{\text{th,max}}$	$P_i^{\text{th,min}}$	RU_i	RD_i
G_1	0.0128	17.82	10.15	100	50	12.50	12.50
G_2	0.0459	15.47	74.33	80	30	10	10
G_3	0.0228	17.82	10.15	100	50	12.50	12.50
G_4	0.0559	15.47	74.33	80	30	10	10
G_5	0.0328	17.82	10.15	100	50	12.50	12.50
G_6	0.0659	15.47	74.33	80	30	10	10

Load forecast data are collected from the PJM Interconnection LLC of North America [28] and are scaled down according to the size of this test system. The historical wind power forecast data are gathered from EIRGRID [29] for the years 2014 to 2017. The wind power forecast error in area 3 is almost two times the average of the forecast error in area 1 and area 2 in both day-ahead and look-ahead time scales. The day-ahead (red line) and look-ahead (black line) net load and the wind power forecast in the corresponding four hours is demonstrated in Fig. 4(b). The load forecast does not change among the time scales here. $P^{C}_{m,t}$, $P^{\text{Rup}}_{m,t}$ and $P^{\text{Rdn}}_{m,t}$ are demonstrated in Fig. 4(c).

2) Basic Scheduling Results

The scheduled outputs of each thermal unit are displayed in Fig. 5(a). Scheduling results show that area 1 is assigned with

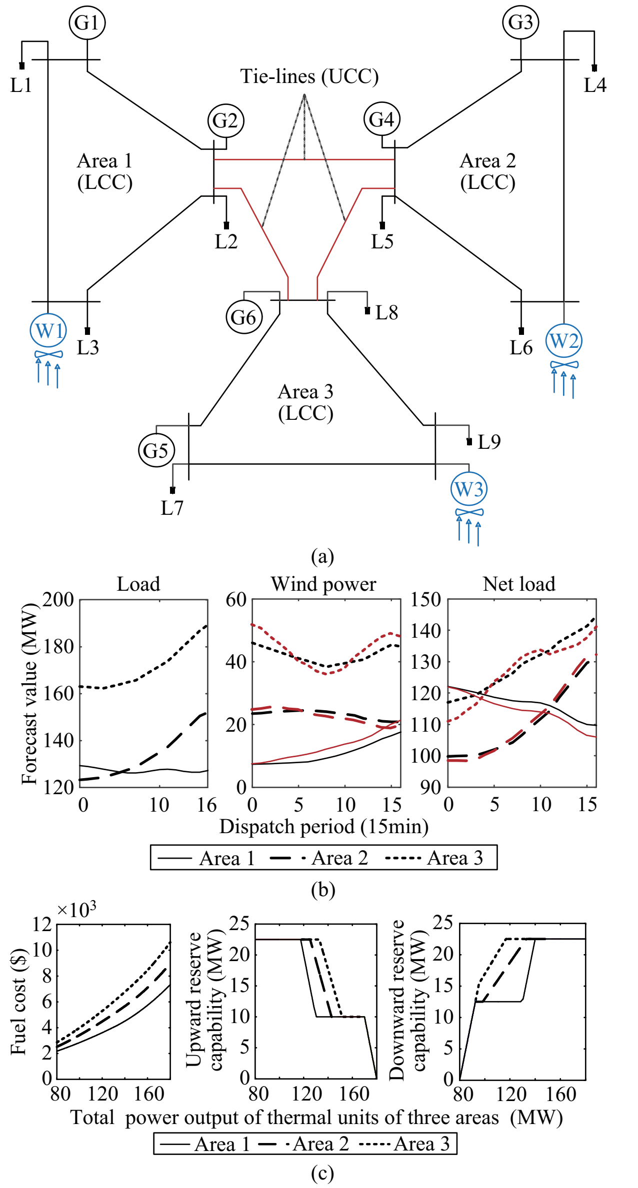

Fig. 4. 9-bus system and its input data. (a) Topological structure of 9-bus system. (b) Load, wind power and net load forecast curves in day-ahead (red line) and look-ahead (black line) time scale. (c) Integrated curves demonstration.

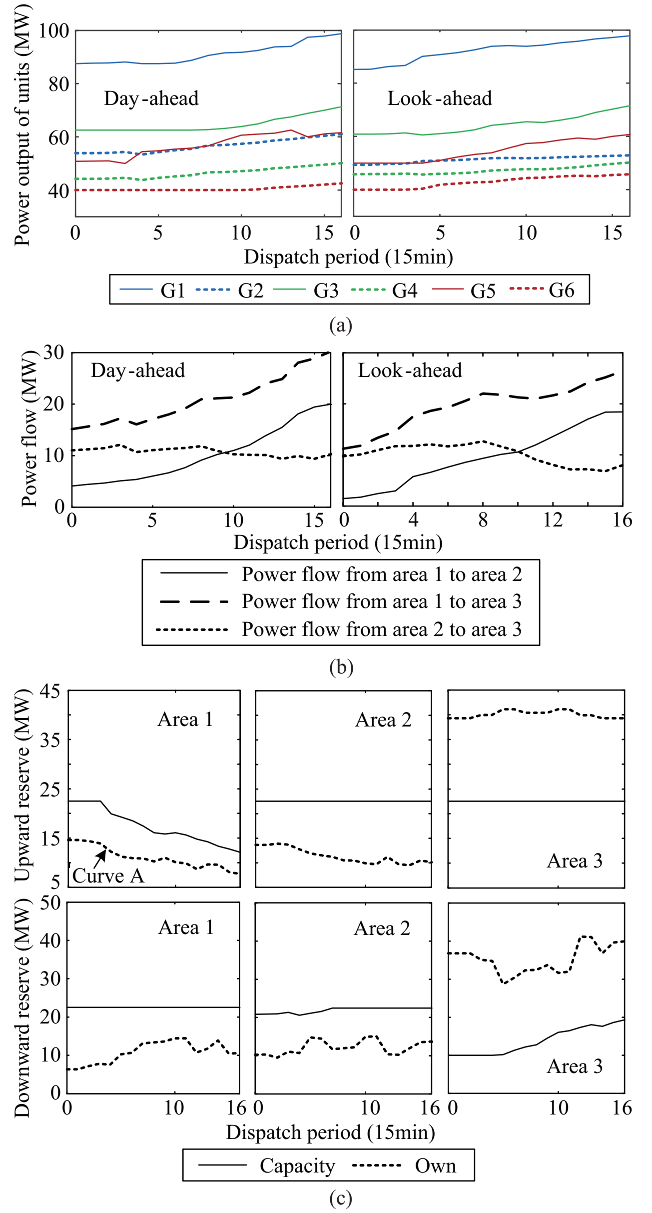

Fig. 5. Basic scheduling results of the 9-bus system. (a) Scheduled total thermal power output. (b) Power flow among three areas. (c) Reserve capacity and own by three areas.

the greatest load because the cheapest fuel costs are in area 1. On the contrary, the thermal units in area 3 have the lowest load in the whole system due to their higher fuel costs. The power flow in the tie-lines is shown in Fig. 5(b). The directions of power flow show that area 1 sends power to other areas and area 3 receives power from outside. In Fig. 5(c), reserve capacity of area m shows the ability of area m to provide reserve. The reserve owned by area m indicates the sum of reserve capacity of area m and the boundary reserve trading volume of area m. Both the upward and downward reserve shows the same trends that area 1 and area 2 provide reserve to area 3. This trend is consistent with the fact that both the positive and the negative wind power forecast errors of the wind farm in area 3 are the largest within the whole system.

Taking upward reserve as an example, Fig. 6 illustrates the effectivity oriented allocation of reserve sources among different dispatch periods. Fig. 6(a) shows that the average ordinate value of the R_m^{LS} in bin 3 under the same abscissa values are almost two times that of the R_m^{LS} in bin 6. This shows that area 1 in dispatch period 1 faces a much higher LS expectation than it does in dispatch period 10 under the same upward reserve. In line with this trend, area 1 owns more upward reserve in dispatch period 1 than it does in dispatch period 10 according to the our schedule results. Fig. 6(b) illustrates the effectivity oriented allocation of reserve sources among areas. According to the comparison of R_m^{LS} in bin 3 of area 1, bin 10 of area 2 and bin 10 of area 3, area 3 obviously faces much higher LS expectations when owning the same amount of upward reserve with area 1 and area 2 in dispatch period 0. This difference indicates that the demand of the upward reserve of area 3 is more urgent than that of

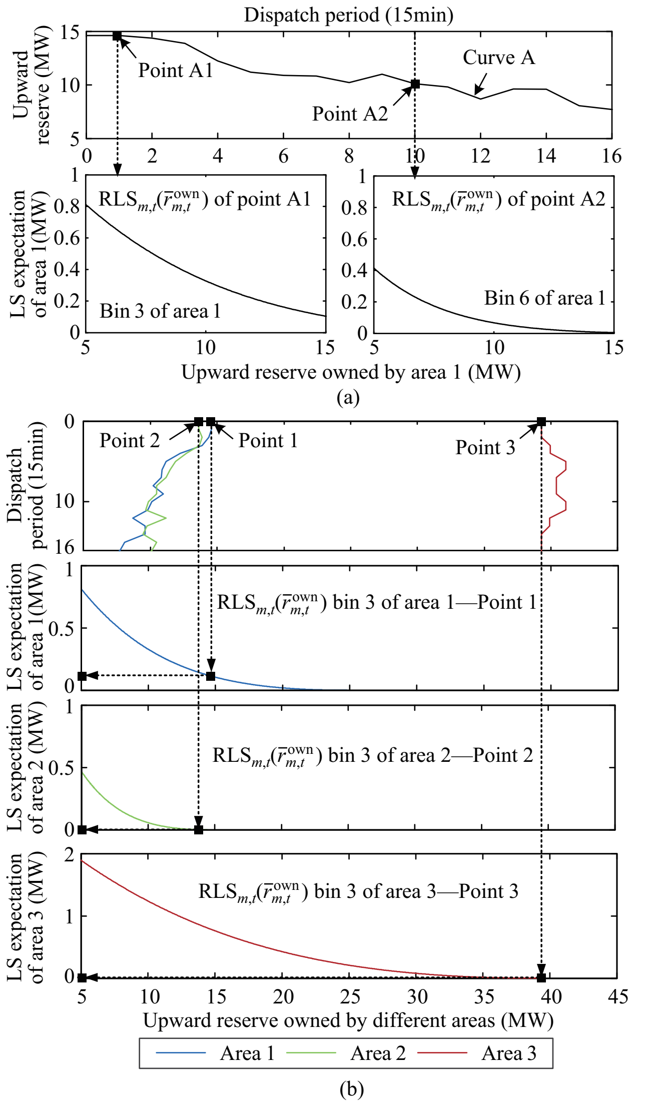

Fig. 6. Effectivity analysis of owning upward reserve among multi-areas and multi-time-periods. (a) Cost-effectivity comparisons among upward reserve owned by area 1 in different dispatch periods. (b) Cost-effectivity comparisons among upward reserve owned by three areas in the same dispatch period.

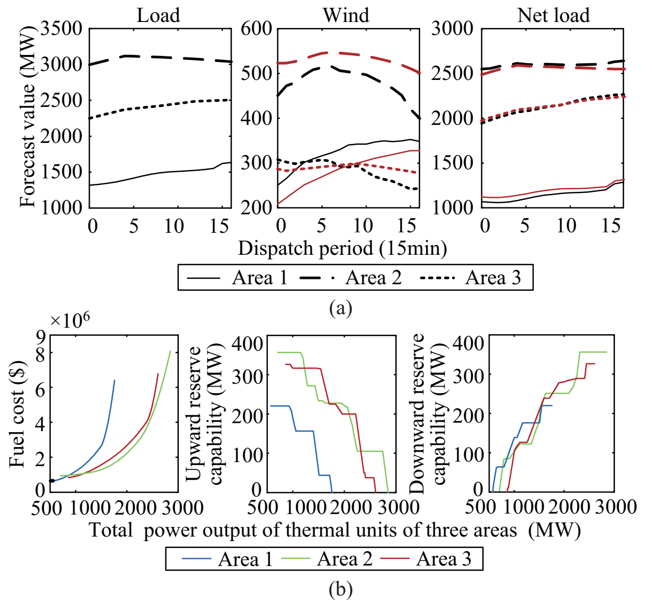

Fig. 7. Input information of the IEEE 118-bus test system. (a) Load, wind power and net load forecast curves day-ahead (red lines) look-ahead (black lines) time scales. (b) Integrated curves demonstratio.

TABLE II
ECONOMIC ANALYSIS OF CENTRALIZED DISPATCH MODEL

Type of cost	Fuel cost ($)	LS cost expectation ($)	WC cost expectation ($)	Total ($)
Area 1	84296	877	161	85334
Area 2	137786	1037	179	139001
Area 3	129244	1069	176	130489
118-bus system	351326	2983	516	354825

TABLE III
ECONOMIC ANALYSIS OF THE PROPOSED MODEL

Type of cost	Fuel cost ($)	LS cost expectation ($)	WC cost expectation ($)	Total ($)
Area 1	84297	878	169	85340
Area 2	137792	1052	183	139127
Area 3	129254	1075	178	130592
118-bus system	351343	3005	530	354878

both areas 1 and 2, which coincides with our schedule results.

B. IEEE 118-bus Test System

1) System and Input Data

The load distribution proportions in the IEEE 118-bus test system [22] are 22.7% in area 1, 41.6% in area 2 and 35.7% in area 3. There are four cross-region tie-lines between area 1 and 2, and five tie-lines between area 2 and 3. Other historical data sources adopted here are consistent with the data used in the 9-bus test system and they are proportionally modified according to their system scale. Three wind farms are located on node 12, node 54 and node 106 [30], with 500 MW, 1000 MW and 500 MW installed capacities respectively. The input information of the 118-bus system is displayed in Fig. 7.

2) Comparison with the Centralized ED Model

The centralized dispatch model is built to verify the accuracy of the proposed information integration method. Compared with the proposed multi-time scale TERA model, the centralized ED model here only removes the hierarchical information exchange portion. The economic analyses of the centralized ED model and the proposed multi-time scale TERA model are shown in Table II and Table III respectively.

By contrast with the two tables above, the economy of the centralized ED model and the proposed multi-time scale TERA model is almost identical with only 0.015% difference in total cost. This gap is primarily due to the numerical calculation. Twenty other sets of input data are also tested in the proposed model and the solution times are demonstrated in Fig. 8. According to the statistical data, the UCC takes an average 8.45 s and the LCC takes an average 2.00 s to solve the corresponding section within the proposed day-ahead TERA model. As for the look-ahead TERA model, the UCC takes an average 2.27 s and the LCC takes an average 1.11 s to finish the optimization process. To sum up, both the calculation precision and the calculation speed of the proposed method and model satisfy engineering requirements.

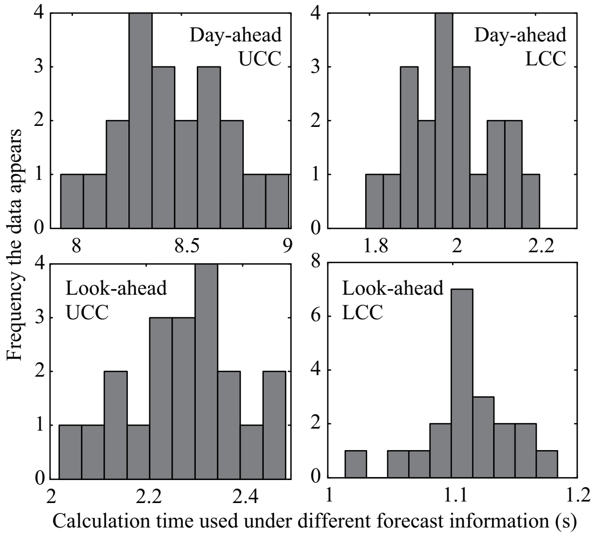

Fig. 8. Statistical data of the calculation time of the proposed model.

V. Conclusion

This paper develops an information integration method for the LCC within a multi-area system to tally with the hierarchical control structure. The method contains three types of relationship curves, namely the $P^{C}_{m,t}$, "$P^{\mathrm{Rup}}_{m,t}$ and $P^{\mathrm{Rdn}}_{m,t}$" and "$R^{\mathrm{LS}}_{m,t}$ and $R^{\mathrm{WC}}_{m,t}$" Based on the uploaded relationship curves, the UCC is able to achieve reasonable allocation of both energy and reserves among the areas without knowing the unit parameters within each area. This method achieves a high quality solution which is close enough to the results of the centralized ED model with full information. Then, this paper designs a multi-time scale TERA model conforming to both the MSCF and the hierarchical control structure adopted in real operations in China. The look-ahead part adjusts the operational points of the thermal units and shares the quantity of energy and reserves among areas on the basis of the day-ahead TERA results. Moreover, the capacity in the tie-lines is also set aside for the sharing reserve, which guarantees the shaving reserve can be delivered when needed. According to the verification results in both 9-bus and 118-bus systems, the proposed multi-time scale TERA model is more than a shortage relieve process but also an efficiency oriented energy and reserve allocation process.

References

[1] X. R. Sun, P. B. Luh, K. W. Cheung, W. Guan, L. D. Michel, S. S. Venkata, and M. T. Miller, "An efficient approach to short-term load forecasting at the distribution level," *IEEE Transactions on Power Systems*, vol. 31, no. 4, pp. 2526–2537, Jul. 2016.

[2] M. Tucci, E. Crisostomi, G. Giunta, and M. Raugi, "A multi-objective method for short-term load forecasting in European countries," *IEEE Transactions on Power Systems*, vol. 31, no. 5, pp. 3537–3547, Sep. 2016.

[3] H. Y. Jin, Z. S. Li, H. B. Sun, Q. L. Guo, and B. Wang, "Coordination on industrial load control and climate control in manufacturing industry under TOU prices," *IEEE Transactions on Smart Grid*, vol. 10, no. 1, pp. 139–152, Jan. 2019.

[4] D. N. Liu, L. Zeng, C. B. Li, K. L. Ma, Y. J. Chen, and Y. J. Cao, "A distributed short-term load forecasting method based on local weather information," *IEEE Systems Journal*, vol. 12, no. 1, pp. 208–215, Mar. 2018.

[5] Y. K. Semero, J. H. Zhang, and D. H. Zheng, "PV power forecasting using an integrated GA-PSO-ANFIS approach and gaussian process regression based feature selection strategy," *CSEE Journal of Power and Energy Systems*, vol. 4, no. 2, pp. 210–218, Jun. 2018.

[6] Z. S. Li, Q. L. Guo, H. B. Sun, and J. H. Wang, "Storage-like devices in load leveling: Complementarity constraints and a new and exact relaxation method," *Applied Energy*, vol. 151, pp. 13–22, Aug. 2015.

[7] X. L. Liu, Y. B. Liu, J. Y. Liu, Y. Xiang, and X. D. Yuan, "Optimal planning of AC-DC hybrid transmission and distributed energy resource system: review and prospects," *CSEE Journal of Power and Energy Systems*, vol. 5, no. 3, pp. 409–422, Sep. 2019.

[8] Q. F. Chen, M. C. Xia, T. Lu, X. C. Jiang, W. X. Liu, and Q. F. Sun, "Short-term load forecasting based on deep learning for end-user transformer subject to volatile electric heating loads," *IEEE Access*, vol. 7, pp. 162697–162707, Nov. 2019.

[9] X. L. Tang, Y. Y. Dai, Q. Liu, X. Y. Dang, and J. Xu, "Application of bidirectional recurrent neural network combined with deep belief network in short-term load forecasting," *IEEE Access*, vol. 7, pp. 160660–160670, Nov. 2019.

[10] J. C. López, M. J. Rider, and Q. W. Wu, "Parsimonious short-term load forecasting for optimal operation planning of electrical distribution systems," *IEEE Transactions on Power Systems*, vol. 34, no. 2, pp. 1427–1437, Mar. 2019.

[11] C. M. Lee and C. N. Ko, "Short-term load forecasting using lifting scheme and ARIMA models," *Expert Systems with Applications*, vol. 38, no. 5, pp. 5902–5911, May. 2011.

[12] N. T. Huang, G. B. Lu, and D. G. Xu, "A permutation importance-based feature selection method for short-term electricity load forecasting using random forest," *Energies*, vol. 9, no. 10, pp. 767, Oct. 2016.

[13] K. Methaprayoon, W. J. Lee, S. Rasmiddatta, J. R. Liao, and R. J. Ross, "Multistage artificial neural network short-term load forecasting engine with front-end weather forecast," *IEEE Transactions on Industry Applications*, vol. 43, no. 6, pp. 1410–1416, Nov. 2007.

[14] W. C. Kong, Z. Y. Dong, Y. W. Jia, D. J. Hill, Y. Xu, and Y. Zhang, "Short-term residential load forecasting based on LSTM recurrent neural network," *IEEE Transactions on Smart Grid*, vol. 10, no. 1, pp. 841–851, Jan. 2019.

[15] T. H. Ouyang, Y. S. He, H. J. Li, Z. Y. Sun, and S. Baek, "Modeling and forecasting short-term power load with copula model and deep belief network," *IEEE Transactions on Emerging Topics in Computational Intelligence*, vol. 3, no. 2, pp. 127–136, Apr. 2019.

[16] Q. Z. Liu, Y. B. Shen, L. Wu, J. Li, L. R. Zhuang, and S. F. Wang, "A hybrid FCW-EMD and KF-BA-SVM based model for short-term load forecasting," *CSEE Journal of Power and Energy Systems*, vol. 4, no. 2, pp. 226–237, Jun. 2018.

[17] H. G. Jiang, Y. C. Zhang, E. Muljadi, J. J. Zhang, and D. W. Gao, "A short-term and high-resolution distribution system load forecasting approach using support vector regression with hybrid parameters optimization," *IEEE Transactions on Smart Grid*, vol. 9, no. 4, pp. 3341–3350, Jul. 2018.

[18] M. R. Haq and Z. Ni, "A new hybrid model for short-term electricity load forecasting," *IEEE Access*, vol. 7, pp. 125413–125423, Sep. 2019.

[19] W. C. Kong, Z. Y. Dong, D. J. Hill, F. J. Luo, and Y. Xu, "Short-term residential load forecasting based on resident behaviour learning," *IEEE Transactions on Power Systems*, vol. 33, no. 1, pp. 1087–1088, Jan. 2018.

[20] K. J. Chen, K. L. Chen, Q. Wang, Z. Y. He, J. Hu, and J. L. He, "Short-term load forecasting with deep residual networks," *IEEE Transactions on Smart Grid*, vol. 10, no. 4, pp. 3943–3952, Jul. 2019.

[21] B. W. Li, J. Zhang, Y. He, Y. Wang, "Short-term load-forecasting method based on wavelet decomposition with second-order gray neural network model combined with ADF Test," *IEEE Access*, vol. 5, pp. 16324–16331, Sep. 2017.

[22] T. E. Huang, Q. L. Guo, H. B. Sun, C. W. Tan, and T. Y. Hu, "A deep learning approach for power system knowledge discovery based on multitask learning," *IET Generation, Transmission & Distribution*, vol. 13, no. 5, pp. 733–740, Mar. 2019.

[23] Y. Wu, J. W. Lei, L. S. Bao, C. Z. Li, "Short-term load forecasting based on improved grey relational analysis and neural network optimized by BAT algorithm," *Automation of Electric Power Systems*, vol. 42, no. 20, pp. 67–72, Oct. 2018.

[24] D. N. Reshef, Y. A. Reshef, H. K. Finucane, S. R. Grossman, G. McVean, P. J. Turnbaugh, E. S. Lander, M. Mitzenmacher, and P. C. Sabeti, "Detecting novel associations in large data sets," *Science*, vol. 334, no. 6062, pp. 1518–1524, Dec. 2011.

[25] A. Basilevsky, *Statistical Factor Analysis and Related Methods: Theory and Applications*. New York: Wiley, 1994, pp. 351–352.

[26] C. García-Martos, J. Rodríguez, and M. J. Sánchez, "Forecasting electricity prices and their volatilities using Unobserved Components," *Energy Economics*, vol. 33, no. 6, pp. 1227–1239, Nov. 2011.
[27] C. García-Martos, J. Rodríguez, and M. J. Sánchez, "Forecasting electricity prices by extracting dynamic common factors: application to the Iberian Market," *IET Generation, Transmission & Distribution*, vol. 6, no. 1, pp. 11–20, Jan. 2012.
[28] K. Nose-Filho, A. D. P. Lotufo, and C. R. Minussi, "Short-term multinodal load forecasting using a modified general regression neural network," *IEEE Transactions on Power Delivery*, vol. 26, no. 4, pp. 2862–2869, Oct. 2011.
[29] Y. Liang, D. X. Niu, and W. C. Hong, "Short term load forecasting based on feature extraction and improved general regression neural network model," *Energy*, vol. 166, pp. 653–663, Jan. 2019.
[30] R. Hu, S. P. Wen, Z. G. Zeng, and T. W. Huang, "A short-term power load forecasting model based on the generalized regression neural network with decreasing step fruit fly optimization algorithm," *Neurocomputing*, vol. 221, pp. 24–31, Jan. 2017.
[31] M. Zeng, S. Xue, Z. J. Wang, X. L. Zhu, and G. Zhang, "Short-term load forecasting of smart grid systems by combination of general regression neural network and least squares-support vector machine algorithm optimized by harmony search algorithm method," *Applied Mathematics & Information Sciences*, vol. 7, no. 1L, pp. 291–298, Feb. 2013.
[32] L. Y. Liu, Y. Zhao, D. L. Chang, J. Y. Xie, Z. Y. Ma, Q. Sun, H. Y. Yin, and R. Wennersten, "Prediction of short-term PV power output and uncertainty analysis," *Applied Energy*, vol. 228, pp. 700–711, Jul. 2018.
[33] K. Li, G. Y. Cheng, X. D. Sun, and Z. B. Yang, "A nonlinear flux linkage model for bearingless induction motor based on GWO-LSSVM," *IEEE Access*, vol. 7, pp. 36558–36567, 2019.
[34] S. Y. Dai, D. X. Niu, and Y. Li, "Daily peak load forecasting based on complete ensemble empirical mode decomposition with adaptive noise and support vector machine optimized by modified grey wolf optimization algorithm," *Energies*, vol. 11, no. 1, pp. 163, Jan. 2018.
[35] L. J. Ge, Y. L. Li, Y. M. Xian, Y. Wang, D. Liang, and J. Yan, "A FA-GWO-GRNN method for short-term photovoltaic output prediction," in *2020 IEEE PES General Meeting*, Montreal, Canada, Aug. 2020.
[36] L. J. Ge, Y. M. Xian, J. Yan, B. Wang, and Z. G. Wang, "A hybrid model for short-term PV output forecasting based on PCA-GWO-GRNN," *Journal of Modern Power Systems and Clean Energy*, vol.8, no.6, pp.1268–1275, Nov. 2020.
[37] S. Mirjalili, S. M. Mirjalili, and A. Lewis, "Grey wolf optimizer," *Advances in Engineering Software*, vol. 69, pp. 46–61, Mar. 2014.
[38] D. Z. Yang, E. Wu, and J. Kleissl, "Operational solar forecasting for the real-time market," *International Journal of Forecasting*, vol. 35, no. 4, pp. 1499–1519, Oct.-Dec. 2019.
[39] D. Reshef, Y. Reshef, P. Sabeti, "P-Value Tables," *maximal information-based nonparametric exploration*. Retrieved February 9, 2020 from http://www.exploredata.net/Downloads/P-Value-Tables.
[40] Z. K. Yi, Y. L. Xu, W. Gu, and W. C. Wu, "A multi-time-scale economic scheduling strategy for virtual power plant based on deferrable loads aggregation and disaggregation," *IEEE Transactions on Sustainable Energy*, vol. 11, no. 3, pp. 1332–1346, Jul. 2020.

Jian Xu (M'08–SM'18) received the B.S. and Ph.D. degrees in Electrical Engineering from Wuhan University, Wuhan, China, in 2002 and 2007, respectively. He is currently a Professor with the School of Electrical Engineering and Automation, Wuhan University. His research interests include power system operation, voltage stability, and wind power control and integration.

Siyang Liao (M'18) received the B.S. and Ph.D. degrees in Electrical Engineering from Wuhan University, Wuhan, China, in 2011 and 2016, respectively. He is currently an Associated Professor with the School of Electrical Engineering and Automation, Wuhan University. His research interests include wind power integration and power system simulation technology.

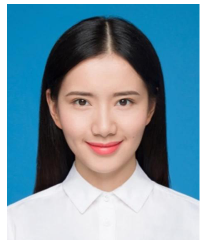

Haiyan Jiang received the B.S. and Ph.D. degrees in Electrical Engineering from Wuhan University, Wuhan, China, in 2012 and 2017, respectively. She is currently a Researcher in the State Grid (Suzhou) Urban Energy Research Institute. Her main research interests include wind power integration, energy and reserve allocation, and multi-time scale economic dispatch.

Danning Zhang received the B.E. degree in Electrical Engineering from the School of Electrical Engineering, Wuhan University, Wuhan, China, in 2016. Her main research interests include power system analysis and automation, energy and reserve allocation, wind power, and multi-time scale economic dispatch.

Yuanzhang Sun (M'99–SM'01) received the Ph.D. degree in Electrical Engineering from Tsinghua University, Beijing, China, in 1988. He is currently a Professor with the School of Electrical Engineering and Automation, Wuhan University, Wuhan, China, and a Chair Professor with the Department of Electrical Engineering and Vice Director of the State Key Laboratory of Power System Control and Simulation, Tsinghua University. His research interests include the areas of power system dynamics and control, wind power, voltage stability and control, and reliability.

Deping Ke received the B.S. degree in Electrical Engineering from Huazhong University of Science and Technology, Wuhan, China, and the Ph.D. degree in Electrical Engineering from Hong Kong Polytechnic University, Hong Kong, China, in 2005 and 2012, respectively. He is currently an Associate Professor with the School of Electrical Engineering and Automation, Wuhan University, Wuhan, China. His research interests include power system dynamics and control, and economical operation of power systems.

Xiong Li received the Ph.D. degree in Electrical Engineering from Tsinghua University, Beijing, China, in 1997. He is currently an Associate Professor with Wuhan University, Wuhan, China. His research interests include power system dynamics and control and WAMS-based closed-loop control systems.

Jun Yang received the Ph.D. degree in Electrical Engineering from Huazhong University of Science and Technology, Wuhan, China, in 2006. He is currently a Professor with Wuhan University, Wuhan, China. His research interests include power system security, electrical vehicles, and smart grid.

Xiaotao Peng received the B.S. degree in Automation Control Engineering and the Ph.D. degree in Electrical Engineering from the Huazhong University of Science and Technology, Wuhan, China, in 1993 and 2006, respectively. He is currently an Associate Professor with the School of Electrical Engineering and Automation, Wuhan University, Wuhan, China. His research interests include power system dynamics and control, and application of energy storage system in power systems.

Liangzhong Yao (SM'12) received the M.Sc. and Ph.D. degrees in Electrical Power Engineering from Tsinghua University, Beijing, China, in 1989 and 1993, respectively. He is currently the Professor with the School of Electrical Engineering and Automation, Wuhan University, Hubei, China. He was a Postdoctoral Research Associate with the University of Manchester (formerly the University of Manchester Institute of Science and Technology), Manchester, U.K., from 1995 to 1999; a Senior Power System Analyst with the Network Consulting Department, ABB U.K., Ltd., from 1999 to 2004; the Department Manager for Network Solutions, Renewables and Smart Grids Technologies with ALSTOM Grid Research & Technology Centre, Stafford, U.K., from 2004 to 2011; the Vice-President with State Grid Electric Power Research Institute (i.e., NARI Group), Nanjing, from 2011 to 2012, and the Vice-President and Honorary Chief Engineer with China Electric Power Research Institute, Beijing, from 2011 to 2018. Dr. Yao is a Chartered Engineer, a Fellow of the IET, and a member of CIGRE. His research interests include hybrid power systems and power system simulation technology.